catalysts

MDPI

*Article*

# Petal-like g-$C_3N_4$ Enhances the Photocatalyst Removal of Hexavalent Chromium

**Huijuan Yu [1,2], Qiang Ma [3], Cuiping Gao [1], Shaohua Liao [1], Yingjie Zhang [1,2,*], Hong Quan [1,2] and Ruiqi Zhai [1,2]**

[1] College of Agriculture and Biological Science, Dali University, Dali 671000, China
[2] Key Laboratory of Ecological Microbial Remediation Technology of Yunnan Higher Education Institutes, Dali University, Dali 671000, China
[3] School of Architecture and Civil Engineering, Chengdu University, Chengdu 610106, China
* Correspondence: yjzhang_dlu@163.com

**Abstract:** The rapid progress of modern industry not only brings convenience to people's lives, but also brings negative effects. Industrial development produces a large amount of waste metal, which brings harm to the environment and human health. Carbon nitride (g-$C_3N_4$) was successfully prepared using the thermal-polymerization method and petal-like g-$C_3N_4$ (CA-g-$C_3N_4$) was impregnated with citric acid (CA). Compared with g-$C_3N_4$, CA-g-$C_3N_4$ showed extremely high photocatalytic activity because the petal-like g-$C_3N_4$ (CA-g-$C_3N_4$) had a larger specific surface area, which increased the active sites on the surface of the photocatalyst and improved the photocatalytic activity. After citric acid treatment, the removal of hexavalent chromium (Cr(VI)) by g-$C_3N_4$ increased from 48% to 93%. The photocatalytic materials were characterized using X-ray diffraction (XRD), scanning electron microscopy (SEM), X-ray photoelectron spectroscopy (XPS), Brunauer–Emmett–Teller (BET) and UV-vis diffuse reflectance spectra (UV-vis). In summary, this study confirmed that citric acid can improve the photocatalytic activity of g-$C_3N_4$ by increasing its specific surface area and the active site of the photocatalytic material so as to achieve the purpose of removing hexavalent chromium from water.

**Keywords:** g-$C_3N_4$; citric acid; petal-like g-$C_3N_4$ (CA-g-$C_3N_4$); hexavalent chromium; photocatalysis



**Citation:** Yu, H.; Ma, Q.; Gao, C.; Liao, S.; Zhang, Y.; Quan, H.; Zhai, R. Petal-like g-$C_3N_4$ Enhances the Photocatalyst Removal of Hexavalent Chromium. *Catalysts* **2023**, *13*, 641. https://doi.org/10.3390/catal13030641

Academic Editors: Zhongzhe Wei and Yutong Gong

Received: 28 February 2023
Revised: 19 March 2023
Accepted: 20 March 2023
Published: 22 March 2023



## 1. Introduction

In the process of modernization, mining, metallurgy and electroplating have also been developed and applied extensively, becoming an important support for economic development in many places. While they promote the development of local economies, the problem of disposing of waste pollutants generated by factories has also arisen. Heavy metal pollution has attracted a great deal of attention as one of the most concerning types of pollution [1–3], and it is harmful to human health and ecosystems in different ways [4,5]. Chromium pollution is a type of heavy metal pollution, and the main source is the electroplating industry. As a surface treatment in major manufacturing industries, the electroplating industry has become an important carrier for the development of modern manufacturing industry. Depending on the different types of processed products, the types of wastewater and treatment methods can be very different. Electroplating wastewater is divided into chromium wastewater, cyanide wastewater and other wastewater in the process of treatment. Cr(VI) and Cr(III) are the main forms of chromium in wastewater [6]. Cr(VI) has strong oxidation and can enter the human body through breathing and contact. In severe cases, it can cause cancer and harm human health [7]. Cr(III) is considered a trace element that our body needs [8]. In order to reduce the harm of Cr(VI) in water systems and human health, various scholars have studied its related removal methods. At present, Cr(VI) is mainly removed using physical [9–11], chemical [12–14] and photocatalytic [15–17] processes. In the process of Cr(VI) removal by physical methods, the equipment used is expensive and the technological process is complex, so the removal effect

of low-concentration pollutants is not ideal. In the chemical removal of Cr(VI), chemical agents are often added to achieve the purpose of reducing Cr(VI) in water. This method can effectively remove Cr(VI). However, due to the difficulty of controlling the dosage of chemical agents, other pollutants will be produced in the process of removing Cr(VI), causing pollution of the environment.

As an emerging industry, photocatalysis is an economical, efficient, non-secondary-polluting, high-removal-efficiency and reusable pollutant-removal technology, which can effectively solve the drawbacks of the original treatment technology. Photocatalysis is widely used in pollution removal [18–20], new energy development [21–23] and other areas. g-$C_3N_4$ is often used to degrade pollutants in water, such as Rhodamine B, ofloxacin and heavy metals such as arsenic. Photocatalysis technology can also be applied in the removal of Cr(VI) [24,25] because of its advantages, such as good thermal stability and low preparation cost [26–28]. It can be used to remove heavy metal contaminants and is easy to prepare. At present, the most commonly used preparation method of g-$C_3N_4$ is the thermal-polymerization method [29,30]. In the process of preparing g-$C_3N_4$ by the calcination method, however, the g-$C_3N_4$ prepared by these methods has the disadvantages of structural accumulation, easy recombination of photogenerated electron–hole pairs, small specific surface area and low photocatalytic activity [31,32].

In order to improve these shortcomings, many scholars have conducted many studies. g-$C_3N_4$ has many modification methods, such as element doping [33,34], morphology regulation [35,36], heterojunction construction [37,38] etc. By modifying g-$C_3N_4$, photocatalysts with high photocatalytic activity can be obtained. Yang et al. [39] used melamine as a precursor to prepare it using the thermal-polymerization method under air atmosphere and obtained oxygen-doped carbon nitride (OCN). The structure of nanoparticles and O-doping have an effect on the structure of graphite. The doped O atom replaces the original N atom in the catalyst, which makes the catalyst have higher electronegativity, thus forming a good superposition effect and strengthening the interaction between catalyst layers. O-doping increases the specific surface area of the catalyst and the active site on the catalyst surface, thus increasing the photocatalytic activity of the photocatalyst. Michela Sturiniet et al. [40] obtained g-$C_3N_4$ by polymerizing dicyandiamide, which greatly improved the removal effect of the catalyst on the antibiotic ofloxacin in water. Mitra Mousavi et al. [41] improved the reduction ability of g-$C_3N_4$ to Cr(VI), and successfully prepared g-$C_3N_4$-nanosheet/$ZnMoO_4$ heterojunction materials by using the calcining-hydrothermal method. This method improves the absorption of visible light by photocatalytic materials and inhibits the recombination of electric charge, thus achieving the purpose of improving the reduction of Cr(VI) by photocatalytic materials. The reducing capacity of the g-$C_3N_4$-nanosheet/$ZnMoO_4$ for Cr(VI) is 3.77 times that of g-$C_3N_4$ nanosheet. Wang et al. [42] prepared petal-like g-$C_3N_4$ by changing the proportion of chlorine doping in order to change the disadvantages of small specific surface area and low light utilization, which increased the specific surface area of the catalyst and effectively improved the photocatalytic activity of g-$C_3N_4$. Wang et al. [43] increased the reaction temperature in the process of preparing graphitic carbon nitride, released more gas in the process, and obtained modified graphitic carbon nitride with a porous network structure. The catalyst not only retained the original complete lamellar structure, but also produced a gauze-like porous structure, which increased the specific surface area of the catalyst surface, thus adsorbing more pollutants and achieving the purpose of improving the removal rate of pollutants. g-$C_3N_4$ can be modified in different ways so as to improve its specific surface area, increase the active sites on the surface of the photocatalyst and improve the photocatalytic activity. In conclusion, the main ways to improve the photocatalytic activity of g-$C_3N_4$ include increasing the specific surface area of the g-$C_3N_4$, increasing the active sites on the catalyst surface and inhibiting the recombination of photogenerated electron–hole pairs.

Given this background, we prepared g-$C_3N_4$ by thermal polycondensation with urea as the precursor system, and successfully prepared flower-like g-$C_3N_4$ with large specific

surface area by adding citric acid, achieving the purpose of the efficient removal of Cr(VI) from water. At the same time, we used XRD, SEM, XPS, BET and UV-vis characterization methods to explore the reaction mechanism. This study provides technical support for the remediation of heavy-metal-polluted water by photocatalysis in the future.

## 2. Results and Discussion

### *2.1. Characterization*

#### 2.1.1. XRD Analysis

The XRD patterns of g-$C_3N_4$ and CA-g-$C_3N_4$ are shown in Figure 1. g-$C_3N_4$ (PDF#87-1526) has two diffraction peaks with 2θ angles of 13.1° and 27.5°, which correspond to crystal planes (100) and (002), respectively. The prepared g-$C_3N_4$ corresponds to the peak value of g-$C_3N_4$ in theory, indicating that g-$C_3N_4$ was successfully synthesized by the calcination method. The XRD pattern of CA-g-$C_3N_4$ (PDF# 87-1526) has two diffraction peaks at 13.1° and 27.5°, corresponding to crystal planes (100) and (002). The position and intensity of the diffraction peaks of g-$C_3N_4$ after citric acid treatment are the same with g-$C_3N_4$, which indicates that the phase composition of g-$C_3N_4$ did not change after citric acid treatment. Furthermore, we confirmed that the increase of the photocatalytic activity of the catalyst in SEM analysis was due to the increase of its specific surface.

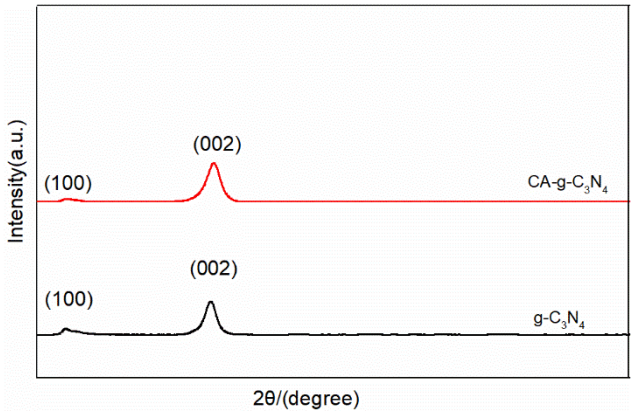


**Figure 1.** XRD patterns of g-$C_3N_4$ and CA-g-$C_3N_4$.

#### 2.1.2. SEM Analysis

The SEM images of g-$C_3N_4$ and CA-g-$C_3N_4$ after the reaction of CA-g-$C_3N_4$ and the EDS element mapping of post-reaction CA-g-$C_3N_4$ (d–h) are shown in Figure 1. In Figure 2a, the pure g-$C_3N_4$ exhibits layers with curved structure at the edges and micropores on some layers. However, the specific surface area of the g-$C_3N_4$ is small because its structure was destroyed under high-temperature calcination, forming the accumulation structure. The SEM image of Figure 2b reflects CA-g-$C_3N_4$ as a chelating agent. Citric acid has a certain dispersion ability. After the addition of citric acid, g-$C_3N_4$ shows a smooth surface structure, and the multiple layered structures form a petal shape, which is conducive to the exposure of materials. At the same time, the image shows that a larger specific surface area provides more active sites, and can effectively improve the photocatalytic activity of the catalyst. Figure 2c displays CA-g-$C_3N_4$ after the reaction. Compared with before the reaction, the layered structure is completely eliminated and the specific surface area is greatly reduced. The reason may be that, during the removal of Cr(VI), a portion of the Cr(VI) accumulated on the surface of the catalyst to form the displayed structure. Figure 2d–g show the mapping of samples after the reaction of CA-g-$C_3N_4$; chromium element was detected in the catalyst. This confirms that the accumulation on the catalyst surface is due to chromium element accumulation. This indicates that citric acid could improve the morphology and structure of g-$C_3N_4$ and enhance the photocatalytic activity.

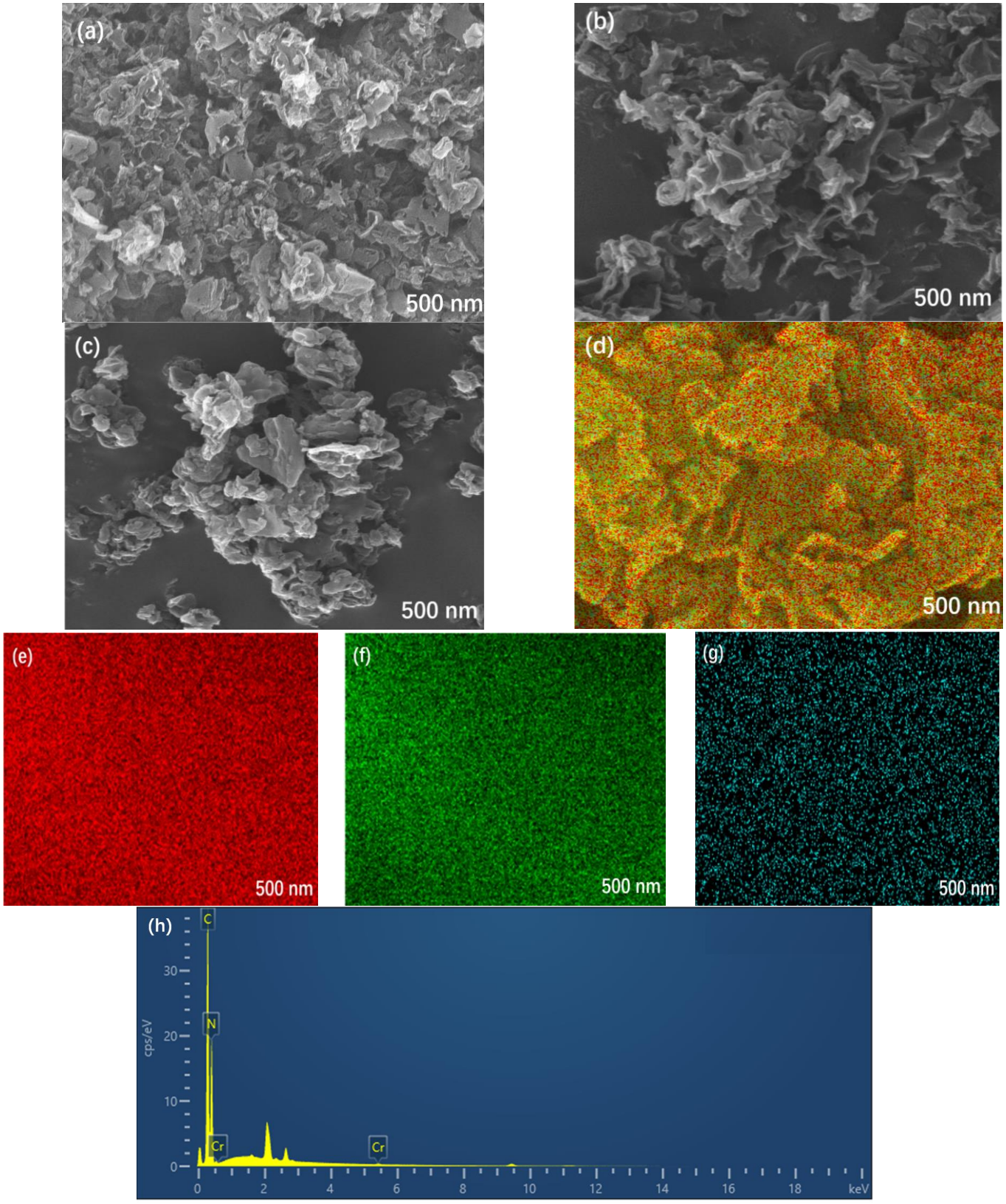


**Figure 2.** SEM images of (**a**) g-$C_3N_4$, (**b**) CA-g-$C_3N_4$ and (**c**) after the reaction of CA-g-$C_3N_4$. EDS element mapping (**d**–**h**) of after the reaction of CA-g-$C_3N_4$.

### 2.1.3. XPS Analysis

In order to determine the elemental composition and chemical bond of g-$C_3N_4$ and CA-g-$C_3N_4$, g-$C_3N_4$ and CA-g-$C_3N_4$ were characterized by XPS, and the results are shown in Figure 3. Figure 3a is a survey of g-$C_3N_4$ and CA-g-$C_3N_4$. In the figure, the composition of g-$C_3N_4$ and CA-g-$C_3N_4$ is the same, which indicates that the addition of citric acid did not change the composition of g-$C_3N_4$. Figure 3b is the C 1s of g-$C_3N_4$ and CA-g-$C_3N_4$. The two fitting peaks of g-$C_3N_4$ are 287.54 and 284.80 eV, respectively. The two fitting peaks of CA-g-$C_3N_4$ are 288.11 and 284.80 eV, respectively, which correspond to N–C=N and C–C in the triazine ring. Figure 3c is the N 1s picture of g-$C_3N_4$ and CA-g-$C_3N_4$. G-$C_3N_4$ has four peaks, which are 398.06, 399.48, 400.52 and 404.00 eV, respectively. CA-g-$C_3N_4$ corresponds to 398.61, 400.14, 401.21 and 404.18 eV, respectively, and C–N=C, N–$C_3$, C–N–H and Π-excitation [44]. Figure 3d shows the O 1s of g-$C_3N_4$ and CA-g-$C_3N_4$, corresponding to 531.89 and 532.50 eV. It can be seen from the XPS results that the addition of citric acid had no effect on the composition and chemical bonds of g-$C_3N_4$.

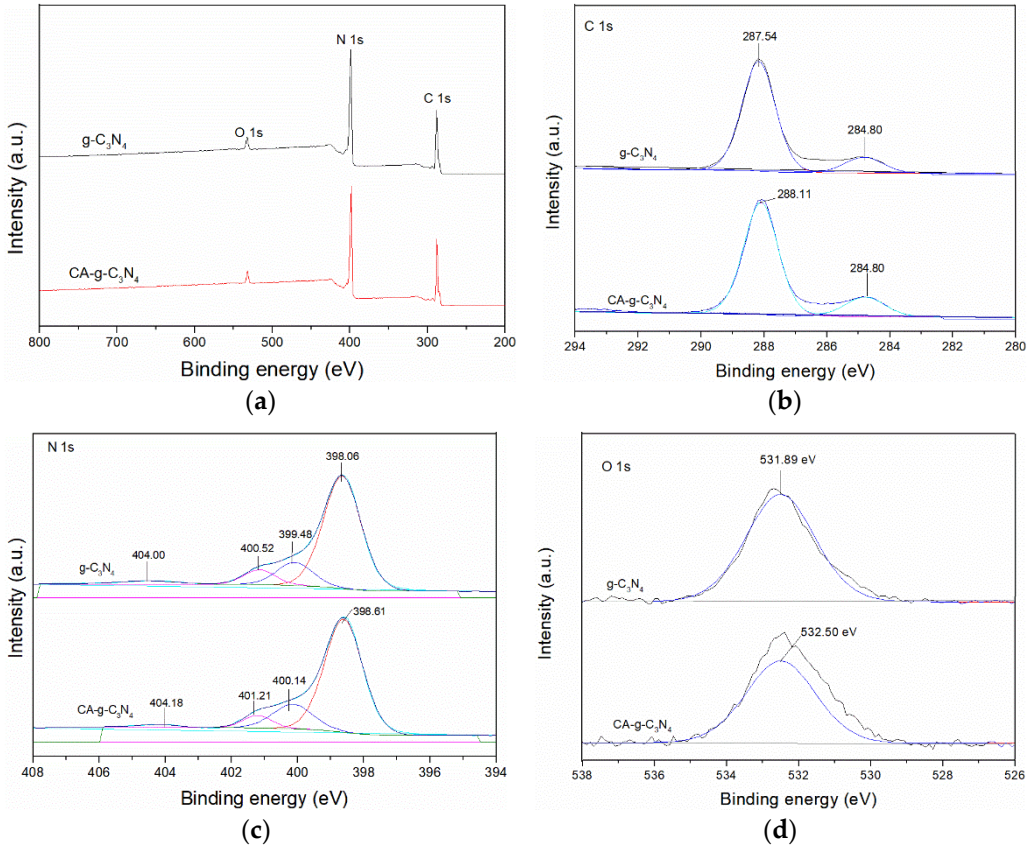


**Figure 3.** XPS of g-$C_3N_4$ and CA-g-$C_3N_4$: (**a**) survey, (**b**) C 1s, (**c**) N 1s and (**d**) O 1s.

### 2.1.4. BET Analysis

The specific surface area, pore volume and pore size of the g-$C_3N_4$, CA-g-$C_3N_4$, post-reaction g-$C_3N_4$ and post-reaction CA-g-$C_3N_4$ are shown in Table 1. The specific surface areas of g-$C_3N_4$, CA-g-$C_3N_4$, post-reaction g-$C_3N_4$ and post-reaction CA-g-$C_3N_4$ were 62.2, 104.0, 48.4 $m^2g^{-1}$ and 58.7 $m^2g^{-1}$, respectively. Pore volumes were 0.3, 0.5, 0.2 and 0.3 $cm^3g^{-1}$, and pore sizes of the three were 18.3, 20.3, 18.3 and 20.2 nm, respectively. It can be found from these data that the specific surface area of g-$C_3N_4$ modified by citric acid was significantly higher than that of pure g-$C_3N_4$, indicating that the addition of citric acid effectively improved the specific surface area and pore size of g-$C_3N_4$. The reason is that the increase of citric acid caused the structure of g-$C_3N_4$ to evacuate and form a larger specific surface area. During the reaction, the photocatalyst can reduce Cr(VI) to Cr(III), it can form $Cr(OH)_3$ colloids in solution and the specific surface area is reduced by deposition

on the surface of the catalyst. We found chrominum on the surface of the material after the reaction through SEM characterization.

**Table 1.** Comparison of specific surface area, pore volumes and pore sizes.

| Sample | $S_{BET}$ ($m^2g^{-1}$) | $V_{pore}$ ($cm^3g^{-1}$) | $d_{pore}$ (nm) |
|---|---|---|---|
| g-$C_3N_4$ | 62.2 | 0.3 | 18.3 |
| CA-g-$C_3N_4$ | 104.0 | 0.5 | 20.3 |
| Post-reaction g-$C_3N_4$ | 48.4 | 0.2 | 18.3 |
| Post-reaction CA-g-$C_3N_4$ | 58.7 | 0.3 | 20.2 |

#### 2.1.5. UV-Vis Analysis

Figure 4 shows the test results of UV-vis characterization of g-$C_3N_4$ and CA-g-$C_3N_4$. g-$C_3N_4$ and CA-g-$C_3N_4$ obtained by this method had excellent light absorption properties in the ultraviolet region. The light absorption range of CA-g-$C_3N_4$ photocatalytic material obtained after citric acid modification of g-$C_3N_4$ was the same as that of the unmodified photocatalytic material. This result indicates that the addition of citric acid had no effect on the structure and chemical composition of g-$C_3N_4$, and the addition of citric acid did not change the light absorption range of g-$C_3N_4$. This proves that the fundamental reason for the increase in the removal rate of Cr(VI) in water by CA-g-$C_3N_4$ is that the addition of citric acid, as an organic acid, effectively changes the microstructure of g-$C_3N_4$, thus increasing the specific surface area of the photocatalyst and the active sites on the catalyst surface, thus improving the photocatalytic activity of the material.

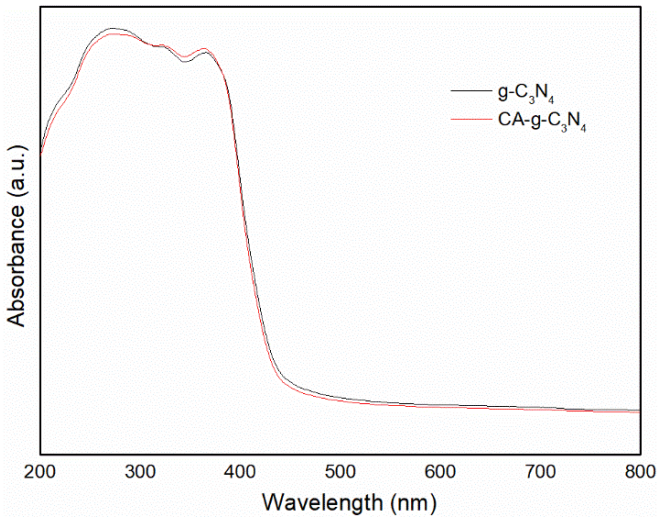


**Figure 4.** UV-vis of g-$C_3N_4$ and CA-g-$C_3N_4$.

### *2.2. g-$C_3N_4$ and CA-g-$C_3N_4$ Performances*

Figure 5 shows the removal rates of Cr(VI) in water by g-$C_3N_4$ and CA-g-$C_3N_4$ under ultraviolet irradiation. The removal rate of Cr(VI) was set under the condition of no light and no catalyst. The catalyst was added to the Cr(VI) solution, and the adsorption–desorption equilibrium was reached by stirring in the dark for 30 min. In this case, the adsorption effect of g-$C_3N_4$ on Cr(VI) was slightly higher than that of CA-g-$C_3N_4$ on Cr(VI). However, after ultraviolet irradiation, the removal rate of Cr(VI) by g-$C_3N_4$ was only 48%, while the removal efficiency of Cr(VI) by CA-g-$C_3N_4$ was up to 93%, showing a higher photocatalytic activity, and the double-beam UV-visible spectrophotometry results for before and after the removal of Cr(VI) are provided in Table 2. The k values of CA-g-$C_3N_4$ and g-$C_3N_4$ were calculated as 0.53753 $min^{-1}$ and 0.38984 $min^{-1}$. In order to more intuitively present the color change of the solution before and after the reaction, we display the solution before and after the reaction. From left to right the color of the solution before

the reaction and that of the solution after g-$C_3N_4$ and CA-g-$C_3N_4$ removal can be seen. The solutions were filtered using membranes. The main reason is that the addition of citric acid effectively dispersed g-$C_3N_4$, increased the specific surface area of the material, improved the active site on the surface of the photocatalyst and thus improved the photocatalytic activity of the photocatalyst.

In order to test the repeatability of the performance of CA-g-$C_3N_4$, we conducted three experiments on the material under the same conditions. The removal rate of Cr(VI) was 93% during the first removal process and 87% during the second and third use processes, indicating that the material has good reusability, as shown in Figure 5d.

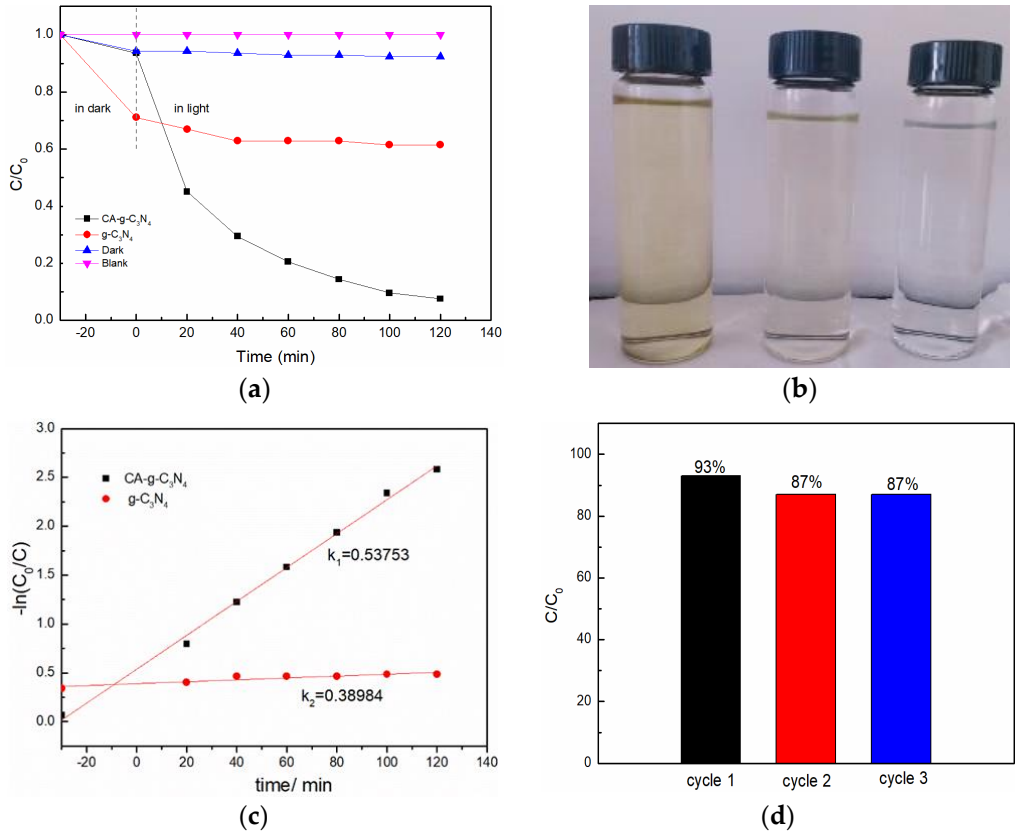


**Figure 5.** Removal rate of g-$C_3N_4$ and CA-g-$C_3N_4$ on Cr(VI) (**a**), the color changes before and after the reaction (**b**), the kinetic constant k of different samples (**c**), the cyclic removal curve of CA-g-$C_3N_4$ (**d**).

**Table 2.** The double beam UV-visible spectrophotometer for before and after removal of chromium (VI).

| Catalytic | | CA-g-$C_3N_4$ | g-$C_3N_4$ | Dark | Blank |
|---|---|---|---|---|---|
| −30 min | A (nm) | 0.145 | 0.112 | 0.146 | 0.150 |
| | removal efficiency (%) | 6.4 | 28.94 | 5.7 | 0 |
| 20 min | A (nm) | 0.074 | 0.106 | 0.146 | 0.149 |
| | removal efficiency (%) | 54.87 | 33.04 | 5.7 | 0 |
| 40 min | A (nm) | 0.051 | 0.100 | 0.145 | 0.150 |
| | removal efficiency (%) | 70.58 | 37.13 | 6.4 | 0 |
| 60 min | A (nm) | 0.038 | 0.100 | 0.144 | 0.150 |
| | removal efficiency (%) | 79.45 | 37.13 | 7.1 | 0 |
| 80 min | A (nm) | 0.029 | 0.100 | 0.144 | 0.151 |
| | removal efficiency (%) | 85.60 | 37.13 | 7.1 | 0 |
| 100 min | A (nm) | 0.022 | 0.098 | 0.143 | 0.152 |
| | removal efficiency (%) | 90.37 | 38.50 | 7.7% | 0 |
| 120 min | A (nm) | 0.019 | 0.098 | 0.143 | 0.150 |
| | removal efficiency (%) | 92.42 | 38.50 | 7.7% | 0 |

In order to further explore the mechanism of increasing photocatalytic activity of CA-g-$C_3N_4$, the main reactive species affecting the photocatalytic reduction of Cr(VI) in CA-g-$C_3N_4$ was identified. 1,4-Benzoquinone (BQ) and Potassium persulfate ($K_2S_2O_8$) were used as scavengers for superoxide radicals ($\cdot O_2^-$) and photo-induced electrons ($e^-$). When BQ was added, the removal rate of Cr(VI) on CA-g-$C_3N_4$ decreased significantly, indicating that $e^-$ was the main active substance in the reaction process. When $K_2S_2O_8$ was added, the removal rate did not decrease significantly, indicating that $\cdot O_2^-$ was not the main active substance, as shown in Figure 6.

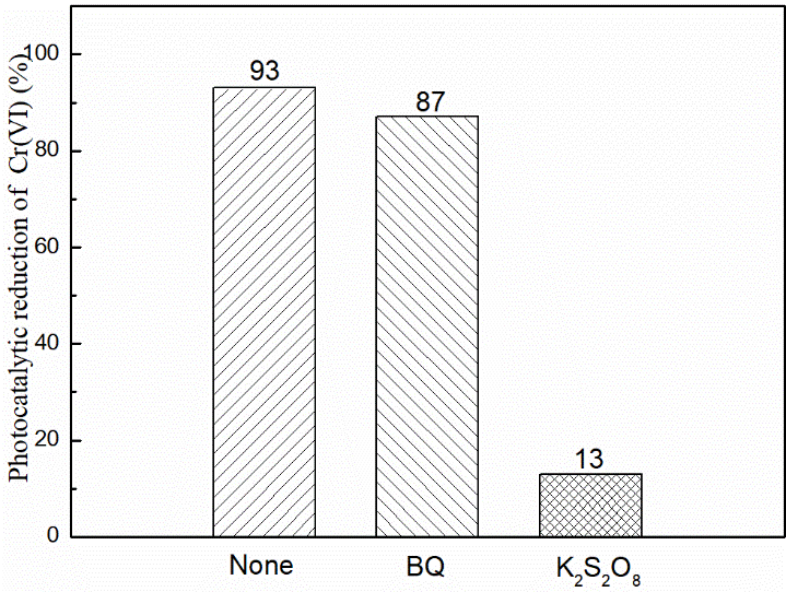


**Figure 6.** Photocatalytic reduction of Cr(VI) experiments with the addition of radical scavenger.

### *2.3. Mechanism of Photocatalysis*

On the basis of the experimental results, characterization data and previous reference materials, we conclude that the reaction mechanism that may be involved in the process of Cr(VI) removal from water by CA-g-$C_3N_4$ is as follows: When the pH value is 1, the main form of chromium is $H_2CrO_4$; when the pH value is 2–6, the form of chromium is $HCrO_4^-$, $Cr_2O_7^{2-}$; when pH > 8, the form of chromium is $CrO_4^{2-}$. Studies have found that when the solution is acidic, the redox potential of Cr(VI) is higher than that of alkaline conditions, and the catalyst surface is positive, which is conducive to the adsorption of Cr(VI) by the catalyst [26,45]. Under the irradiation of ultraviolet light on the catalyst surface, the CA-g-$C_3N_4$ surface is excited to produce photogenerated electrons ($e^-$) and holes ($h^+$) As shown in Equation (1), the photogenerated electron ($e^-$) reduces Cr(VI) to Cr(III). As shown in Equation (2), the hole ($h^+$) reacts with $H_2O$ to form ·OH and $O_2$. As shown in Equation (3), under acidic conditions, the surface of the catalyst is positively charged, which is conducive to the catalyst reduction of Cr(VI), and the redox potential under this condition is higher than that under alkaline conditions. The toxicity of Cr(VI) is greatly reduced by reducing Cr(III), and thus the purpose of degrading heavy metal pollution is achieved. The reaction mechanism is shown in Figure 7.

$$\text{CA-g-}C_3N_4 + hv \rightarrow h^+ + e^- \quad (1)$$

$$CrO_4^{2-} + 8H^+ + 3e^- \rightarrow Cr^{3+} + 4H_2O \quad (2)$$

$$h^+ + H_2O \rightarrow \cdot OH + O_2 \quad (3)$$

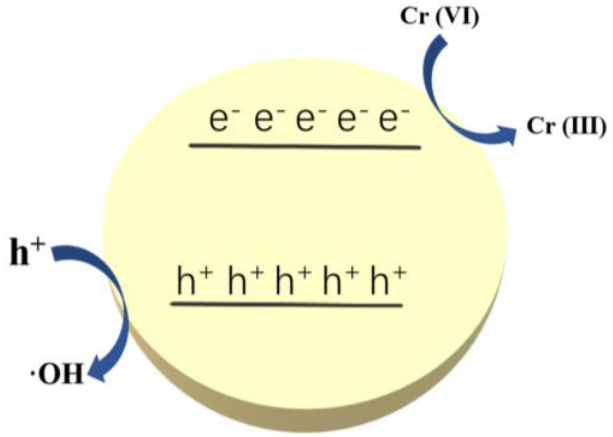


**Figure 7.** The mechanism of photocatalytic CA-g-$C_3N_4$ removal of Cr(VI).

## 3. Materials and Methods

### *3.1. Materials*

Urea ($H_2NCONH_2$) and Citric Acid ($C_6H_8O_7 \cdot H_2O$) were purchased from ZhiYuan chemical reagent company (Tianjin, China). Both were analytical reagents. Hydrochloric acid (HCl) and sodium hydroxide (NaOH) were bought from Xilong Co., Ltd. (Guangzhou, China), where HCl was the guarantee reagent and NaOH was the analytical reagent.

### *3.2. Preparation of g-$C_3N_4$*

In this study, urea was used as the precursor to prepare carbon nitride (g-$C_3N_4$) by thermal polymerization. The specific preparation methods are as follows. An amount of 20 g urea is placed in a covered crucible and sealed with tin foil to achieve an anoxic environment, and then placed in a Muffle furnace. The Muffle furnace temperature is heated to 550 °C at the heating rate of 5 °C/min, and the urea is calcined at the changing temperature for 4 h. Then, the urea is cooled slowly until the temperature reaches room temperature. Then, the material is taken out and a yellow material with low quality is obtained. This yellow material is finely ground in an agate mortar to produce g-$C_3N_4$ powder, which is bagged for future use.

### *3.3. Preparation of CA/g-$C_3N_4$*

CA-g-$C_3N_4$ is prepared by modifying g-$C_3N_4$ by soaking it with citric acid. The specific preparation method is as follows. First, 2 g citric acid (CA) is dissolved in 50 mL deionized water, which is thoroughly mixed to obtain a certain concentration of citric acid solution. Then, g-$C_3N_4$ (2 g) is dissolved in 20 mL citric acid and stirred to fully dissolve g- $C_3N_4$ and citric acid into solution, followed by soaking at room temperature for 24 h to obtain modified g-$C_3N_4$. The obtained g-$C_3N_4$ soaked in citric acid is washed with deionized water and filtered until the pH value of the filtered solution is neutral. The solid parts left after filtering are dried at 60 °C for 12 h to obtain blocky materials, which are fully ground with an agate mortar to obtain yellow powdery CA-g-$C_3N_4$, which is bagged for use.

### *3.4. Characterization*

X-ray diffraction (XRD, Smart Lab SE, Rigaku Corp., Tokyo, Japan) was used to analyze and characterize the phase composition and lattice parameters of g-$C_3N_4$ and CA-g-$C_3N_4$. The test conditions were as follows: Cu target was used, the acceleration voltage was 40 kV, and the current was 40 mA.

A scanning electron microscope (SEM, TESCAN MIRA LMS, TESCAN CHINA, Ltd., Shangai, China) was used to characterize the microstructure of the catalysts. A narrow focused high-energy electron beam was used to scan the sample, and physical information was excited through the interaction between the beam and the substance. X-ray photo-

electron spectroscopy (XPS, Thermo Scientific K-Alpha, Thermo Fisher Scientific Co., Ltd., Shanghai, China) was used to characterize the elemental composition, content and valence states of the catalyst. The light source used was Al Kα. The Brunauer-Emmett-Teller (BET, Micromeritics ASAP2460, Micromeritics Corp., Norcross, GA, USA) $N_2$ adsorption–desorption method was used to characterize the specific surface area and pore size of the samples. UV-vis diffuse reflectance spectra (UV-vis DRS, UV-3600i Plus, Shimadzu Corp., Kyoto, Japan) were used to test the light absorption properties of the samples.

### *3.5. Photocatalytic Tests*

The performance of photocatalyst g-$C_3N_4$ and CA-g-$C_3N_4$ was tested using UV-visible spectrophotometry to measure the absorbance of Cr(VI) before and after the reaction, and the removal effect of Cr(VI) was judged by calculation. The test method of this experiment was as follows: 100 mL Cr(VI) solution with a concentration of 20 mg·$L^{-1}$ and a pH value of 2 was prepared in advance and placed in a quartz reactor; 50 mg photocatalyst g-$C_3N_4$ or CA-g-$C_3N_4$ was added; a rotor was added into the solution and it was stirred through magnetic force to make it evenly mixed. At room temperature, the solution was stirred in the dark for 30 min to achieve adsorption–desorption equilibrium between the solution and the photocatalyst so as to facilitate the subsequent judgment of the photocatalytic activity of the photocatalytic materials. After dark reaction for 30 min, the UV light source was turned on to irradiate the solution, and the water circulation was turned on to control the reaction temperature. When the total irradiation time of the UV lamp was 20, 40, 60, 80, 100 and 120 min, respectively, 2 mL of the reaction solution was taken out, filtered with a biofiltration membrane and 0.5 mL of the filtered solution was taken out for absorbance testing. The solution was not put back each time after removal. According to the absorbance of the solutions obtained at different time periods, the corresponding solution concentration could be calculated, and the above solution concentration and the original solution concentration could be calculated to obtain the removal effect of Cr(VI) in water at each time period by the photocatalyst.

## 4. Conclusions

In this study, the preparation methods of g-$C_3N_4$ and CA-g-$C_3N_4$ photocatalytic material modified by citric acid were studied, and the reaction mechanism involved in the removal of Cr(VI) from water by photocatalyst was explored. g-$C_3N_4$ was prepared by thermal-polymerization and modified by citric acid solution. After modification, CA-g-$C_3N_4$ was obtained. As an organic acid, citric acid has a dispersive effect. After citric acid is added to g-$C_3N_4$, it can be effectively dispersed, which solves the deficiency of the structure accumulation of g-$C_3N_4$ prepared by thermal condensation. By studying the removal effects of different photocatalytic materials on Cr(VI) in water, it was determined that the photocatalytic activity of g-$C_3N_4$ modified by citric acid was effectively improved. The phase composition of g-$C_3N_4$ before and after citric acid modification was determined by XRD, XPS and UV-vis. The crystal structure and light absorption range did not change, indicating that the addition of citric acid did not change the chemical properties of g-$C_3N_4$. However, SEM and BET showed that, compared with g-$C_3N_4$, CA-g-$C_3N_4$ obtained after citric acid modification had a more porous microstructure with significantly larger specific surface area and pore size, which proved that the addition of citric acid effectively dispersed g-$C_3N_4$ and changed its morphology and structure. By increasing its specific surface area, the number of active sites on the material surface was increased. The contact area between Cr(VI) and the photocatalyst was larger, and the removal rate was increased. The ability of g-$C_3N_4$ modified with citric acid to efficiently remove Cr(VI) from water fully proves that morphology control can improve the photocatalytic activity of materials, and provides a new idea for the removal of heavy metals and other pollutants by photocatalytic technology in the future.

**Author Contributions:** All authors contributed to the study conception and design. Methodology and writing—original draft preparation were performed by H.Y.; Writing—Reviewing, editing, and conceptualization were performed by Q.M.; Data curation was performed by C.G.; Validations were performed by S.L.; Investigation and funding acquisition were performed by Y.Z.; Writing—Reviewing and editing were performed by H.Q.; Data curation was performed by R.Z. All authors have read and agreed to the published version of the manuscript.

**Funding:** This work was supported by the Basic Research Project of Yunnan Province Science and Technology Department (grant number: 202201AU070004), the Yunnan Province Education Department Scientific Research Fund Project (grant number: 2023J0959; 2023Y1049), and the Research Program of Yunnan Provincial Science and Technology Department (grant number: 202101BA070001-079).

**Data Availability Statement:** The datasets generated and/or analyzed during the current study are available from the corresponding author on reasonable request.

**Conflicts of Interest:** The authors declare no conflict of interest.

## References

1. Xiang, M.; Li, Y.; Yang, J.; Lei, K.; Li, Y.; Li, F.; Zheng, D.; Fang, X.; Cao, Y. Heavy metal contamination risk assessment and correlation analysis of heavy metal contents in soil and crops. *Environ. Pollut.* **2021**, *278*, 2069–7491. [CrossRef]
2. Sonia, G.; David, W.G.; Sreekrishnan, T.R.; Ahammad, S.Z. Heavy metal and antibiotic resistance in four Indian and UK rivers with different levels and types of water pollution. *Sci. Total Environ.* **2023**, *857*, 159059.
3. Yu, H.; Zhang, Y.; Quan, H.; Zhu, D.; Liao, S.; Gao, C.; Yang, R.; Zhang, Z.; Ma, Q. Simultaneous catalytic oxidation of $Hg^0$ and $AsH_3$ over Fe-Ce co-doped $TiO_2$ catalyst under low temperature and reducing atmosphere. *RSC Adv.* **2023**, *13*, 3958–3970. [CrossRef]
4. Chowdhury, S.; Mazumder, M.J.; Al-Attas, O.; Husain, T. Heavy metals in drinking water: Occurrences, implications, and future needs in developing countries. *Sci. Total Environ.* **2016**, *569–570*, 476–488. [CrossRef] [PubMed]
5. Fu, Z.; Xi, S. The effects of heavy metals on human metabolism. *Toxicol. Mech. Methods* **2020**, *30*, 167–176. [CrossRef]
6. Liang, J.; Huang, X.; Yan, J.; Li, Y.; Zhao, Z.; Liu, Y.; Ye, J.; Wei, Y. A review of the formation of Cr (VI) via Cr (III) oxidation in soils and groundwater. *Sci. Total Environ.* **2021**, 774. [CrossRef]
7. Prasad, S.; Yadav, K.K.; Kumar, S.; Gupta, N.; Cabral-Pinto, M.M.; Rezania, S.; Radwan, N.; Alam, J. Chromium contamination and effect on environmental health and its remediation: A sustainable approaches. *J. Environ. Manag.* **2021**, *285*, 112174. [CrossRef]
8. Ukhurebor, K.E.; Aigbe, U.O.; Onyancha, R.B.; Nwankwo, W.; Osibote, O.A.; Paumo, H.K.; Ama, O.M.; Adetunji, C.O.; Siloko, I.U. Effect of hexavalent chromium on the environment and removal techniques: A review. *J. Environ. Manag.* **2021**, *280*, 111809. [CrossRef]
9. Cui, B.; Chen, Z.; Wang, F.; Zhang, Z.; Dai, Y.; Guo, D.; Liang, W.; Liu, Y. Facile Synthesis of Magnetic Biochar Derived from Burley Tobacco Stems towards Enhanced Cr(VI) Removal: Performance and Mechanism. *Nanomaterials* **2022**, *12*, 678. [CrossRef] [PubMed]
10. Jiang, W.; Cai, Q.; Xu, W.; Yang, M.; Cai, Y.; Dionysiou, D.D.; O'Shea, K.E. Cr(VI) Adsorption and Reduction by Humic Acid Coated on Magnetite. *Environ. Sci. Technol.* **2014**, *48*, 8078–8085. [CrossRef] [PubMed]
11. Shi, S.; Yang, J.; Liang, S.; Li, M.; Gan, Q.; Xiao, K.; Hu, J. Enhanced Cr(VI) removal from acidic solutions using biochar modified by $Fe_3O_4$@$SiO_2$-$NH_2$ particles. *Sci. Total Environ.* **2018**, *628–629*, 499–508. [CrossRef] [PubMed]
12. Jiang, B.; Gong, Y.; Gao, J.; Sun, T.; Liu, Y.; Oturan, N.; Oturan, M. The reduction of Cr (VI) to Cr (III) mediated by environmentally relevant carboxylic acids: State-of-the-art and perspectives. *J. Hazard. Mater.* **2019**, *365*, 205–226. [CrossRef]
13. Zhang, B.; Wang, Z.; Shi, J.; Don, H. Sulfur-based mixotrophic bio-reduction for efficient removal of chromium (VI) in groundwater. *Geochim. Et Cosmochim. Acta* **2020**, *268*, 296–309. [CrossRef]
14. Liu, F.; Hua, S.; Wang, C.; Qiu, M.; Jin, L.; Hu, B. Adsorption and reduction of Cr(VI) from aqueous solution using cost-effective caffeic acid functionalized corn starch. *Chemosphere* **2021**, *279*, 130539. [CrossRef]
15. Zhao, W.; Li, J.; Dai, B.; Cheng, Z.; Xu, J.; Ma, K.; Zhang, L.; Sheng, N.; Mao, G.; Wu, H.; et al. Simultaneous removal of tetracycline and Cr(VI) by a novel three-dimensional AgI/$BiVO_4$ p-n junction photocatalyst and insight into the photocatalytic mechanism. *Chem. Eng. J.* **2019**, *369*, 716–725. [CrossRef]
16. Ge, T.; Jiang, Z.; Shen, L.; Li, J.; Lu, Z.; Zhang, Y.; Wang, F. Synthesis and application of $Fe_3O_4$/$FeWO_4$ composite as an efficient and magnetically recoverable visible light-driven photocatalyst for the reduction of Cr (VI). *Sep. Purif. Technol.* **2021**, *263*, 118401. [CrossRef]
17. Li, L.; Gao, H.; Liu, G.; Wang, S.; Yi, Z.; Wu, X.; Yang, H. Synthesis of carnation flower-like $Bi_2O_2CO_3$ photocatalyst and its promising application for photoreduction of Cr(VI). *Adv. Powder Technol.* **2022**, *33*, 103481. [CrossRef]
18. Xing, Z.; Zhang, J.; Cui, J.; Yin, J.; Zhao, T.; Kuang, J.; Xiu, Z.; Wan, N.; Zhou, W. Recent advances in floating $TiO_2$-based photo-catalysts for environmental application. *Appl. Catal. B Environ.* **2018**, *225*, 452–467. [CrossRef]

19. Lu, Z.; Peng, J.; Song, M.; Liu, Y.; Liu, X.; Huo, P.; Dong, H.; Yuan, S.; Ma, Z.; Han, S. Improved recyclability and selectivity of environment-friendly MFA-based heterojunction imprinted photocatalyst for secondary pollution free tetracycline orientation degradation. *Chem. Eng. J.* **2019**, *360*, 1262–1276. [CrossRef]
20. Senasu, T.; Chankhanittha, T.; Hemavibool, K.; Nanan, S. Visible-light-responsive photocatalyst based on ZnO/CdS nanocomposite for photodegradation of reactive red azo dye and ofloxacin antibiotic. *Mater. Sci. Semicond. Process.* **2021**, *123*, 105558. [CrossRef]
21. Iwashina, K.; Iwase, A.; Ng, Y.H.; Amal, R.; Kudo, A. Z-schematic water splitting into $H_2$ and $O_2$ using metal sulfide as a hydro-gen-evolving photocatalyst and reduced graphene oxide as a solid-state electron mediator. *J. Am. Chem. Soc.* **2015**, *137*, 604–607. [CrossRef]
22. Wu, Y.; Wang, P.; Zhu, X.; Zhang, Q.; Wang, Z.; Liu, Y.; Zou, G.; Dai, Y.; Whangbo, M.; Huang, B. Composite of $CH_3NH_3PbI_3$ with Reduced Graphene Oxide as a Highly Efficient and Stable Visible-Light Photocatalyst for Hydrogen Evolution in Aqueous HI Solution. *Adv. Mater.* **2018**, *30*, 1704342. [CrossRef]
23. Fei, T.; Qin, C.; Zhang, Y.; Dong, G.; Wang, Y.; Zhou, Y.; Cui, M. A 3D peony-like sulfur-doped carbon nitride synthesized by self-assembly for efficient photocatalytic hydrogen production. *Int. J. Hydrogen Energy* **2021**, *46*, 20481–20491. [CrossRef]
24. Li, X.; Lv, X.; Li, N.; Wu, J.; Zheng, Y.-Z.; Tao, X. One-step hydrothermal synthesis of high-percentage 1T-phase $MoS_2$ quantum dots for remarkably enhanced visible-light-driven photocatalytic $H_2$ evolution. *Appl. Catal. B Environ.* **2019**, *243*, 76–85. [CrossRef]
25. Arputharaj, E.; Kumar, A.S.K.; Tseng, W.; Jiang, S.; Huang, Y.; Dahms, H.-U. Self-Assembly of poly (ethyleneimine)-modified g-$C_3N_3$ Nanosheets with lysozyme fibrils for chromium detoxification. *Langmuir* **2021**, *37*, 7147–7155. [CrossRef] [PubMed]
26. Kumar, A.S.K.; You, J.; Tseng, W.; Dwivedi, G.D.; Rajesh, N.; Jiang, S.; Tseng, W. Magnetically separable nano-spherical g-$C_3N_4$@$Fe_3O_4$ as a recyclable viable material for chromium adsorption and visible light driven catalytic re-duction of aromatic nitro compounds. *ACS Sustain. Chem. Eng.* **2019**, *7*, 6662–6671. [CrossRef]
27. Wang, S.; Li, D.; Sun, C.; Yang, S.; Guan, Y.; He, H. Synthesis and characterization of g-$C_3N_4$/$Ag_3VO_4$ composites with signifi-cantly enhanced visible-light photocatalytic activity for triphenylmethane dye degradation. *Appl. Catal. B Environ.* **2014**, *144*, 885–892. [CrossRef]
28. Yan, D.; Wu, X.; Pei, J.; Wu, C.; Wang, X.; Zhao, H. Construction of g-$C_3N_4$/$TiO_2$/Ag composites with enhanced visible-light photocatalytic activity and antibacterial properties. *Ceram. Int.* **2020**, *46*, 696–702. [CrossRef]
29. Sun, H.; Guo, F.; Pan, J.; Huang, W.; Wang, K.; Shi, W. One-pot thermal polymerization route to prepare N-deficient modified g-$C_3N_4$ for the degradation of tetracycline by the synergistic effect of photocatalysis and persulfate-based advanced oxidation process. *Chem. Eng. J.* **2020**, *406*, 126844. [CrossRef]
30. Wang, X.; Zhou, C.; Shi, R.; Liu, Q.; Waterhouse, G.I.N.; Wu, L.; Tung, C.-H.; Zhang, T. Supramolecular precursor strategy for the synthesis of holey graphitic carbon nitride nanotubes with enhanced photocatalytic hydrogen evolution performance. *Nano Res.* **2019**, *12*, 2385–2389. [CrossRef]
31. Guo, S.; Tang, Y.; Xie, Y.; Tian, C.; Feng, Q.; Zhou, W.; Jiang, B. P-doped tubular g-C3N4 with surface carbon defects: Universal synthesis and enhanced visible-light photocatalytic hydrogen production. *Appl. Catal. B Environ.* **2017**, *218*, 664–671. [CrossRef]
32. Lu, M.; Li, Q.; Zhang, C.; Fan, X.; Li, L.; Dong, Y.; Chen, G.; Shi, H. Remarkable photocatalytic activity enhancement of $CO_2$ conversion over 2D/2D g-$C_3N_4$/$BiVO_4$ Z-scheme heterojunction promoted by efficient interfacial charge transfer. *Carbon* **2020**, *160*, 342–352. [CrossRef]
33. Mohamed, S.; Chen, C.; Chen, C.; Hu, S.; Liu, R. High-performance lithium-ion battery and symmetric supercapacitors based on $FeCo_2O_4$ nanoflakes electrodes. *ACS Appl. Mater. Interfaces* **2014**, *6*, 22701–22708. [CrossRef]
34. Li, D.; Wen, C.; Huang, J.; Zhong, J.; Chen, P.; Liu, H.; Wang, Z.; Liu, Y.; Lv, W.; Liu, G. High-efficiency ultrathin porous phosphorus-doped graphitic carbon nitride nanosheet photocatalyst for energy production and environmental remediation. *Appl. Catal. B Environ.* **2022**, *307*, 121099. [CrossRef]
35. Li, B.; Fang, Q.; Si, Y.; Huang, T.; Huang, W.-Q.; Hu, W.; Pan, A.; Fan, X.; Huang, G.-F. Ultra-thin tubular graphitic carbon Nitride-Carbon Dot lateral heterostructures: One-Step synthesis and highly efficient catalytic hydrogen generation. *Chem. Eng. J.* **2020**, *397*. [CrossRef]
36. Dong, X.; Huang, X.; Wang, D.; Lei, Y.; Han, J.; Liang, X.; Wei, Q. Constructing crystalline needle-mushroom-like/amorphous nanosheet carbon nitride homojunction by molten salt method for photocatalytic degradation of tetracycline hydrochloride. *J. Mater. Sci. Mater. Electron.* **2022**, *33*, 6043–6058. [CrossRef]
37. Viet, P.; Nguyen, T.; Bui, D.; Thi, C. Combining $SnO_{2-x}$ and g-$C_3N_4$ nanosheets toward S-scheme heterojunction for high se-lectivity into green products of NO. *J. Mater.* **2022**, *8*, 1–8.
38. Dong, F.; Zhao, Z.; Xiong, T.; Ni, Z.; Zhang, W.; Sun, Y.; Ho, W.-K. In Situ Construction of g-C3N4/g-C3N4 Metal-Free Heterojunction for Enhanced Visible-Light Photocatalysis. *ACS Appl. Mater. Interfaces* **2013**, *5*, 11392–11401. [CrossRef]
39. Yan, Z.; Yang, M.; Chen, Y.; Li, T.; Jing, Q.; Liu, P. Hydroxyl-Rich Porous Silica Nanosheets Decorated with Oxygen-Doped Carbon Nitride Nanoparticles for Photocatalytic Degradation of Rhodamine B. *ACS Appl. Nano Mater.* **2022**, *5*, 818–831. [CrossRef]
40. Sturini, M.; Speltini, A.; Maraschi, F.; Vinci, G.; Profumo, A.; Pretali, L.; Albini, A.; Malavasi, L. g-$C_3N_4$-promoted degradation of ofloxacin antibiotic in natural waters under simulated sunlight. *Environ. Sci. Pollut. Res.* **2017**, *24*, 4153–4161. [CrossRef]
41. Mousavi, M.; Moradian, S.; Pourhakkak, P.; Zhang, G.; Habibi, M.M.; Madadi, M.; Ghasemi, J.B. Fabrication of S-scheme heterojunction g-$C_3N_4$-nanosheet/$ZnMoO_4$ nanocomposite with high efficiency in photocatalytic $N_2$ fixation and Cr(VI) detoxification. *J. Mater. Sci.* **2022**, *57*, 9145–9163. [CrossRef]

42. Wang, D.; Huang, X.; Huang, Y.; Yu, X.; Lei, Y.; Dong, X.; Su, Z. Self-assembly synthesis of petal-like Cl-doped g-$C_3N_4$ nanosheets with tunable band structure for enhanced photocatalytic activity. *Colloids Surf. A Physicochem. Eng. Asp.* **2021**, *611*, 125780. [CrossRef]
43. Wang, D.; Huang, Y.; Yu, X.; Huang, X.; Zhong, Y.; Huang, X.; Liu, Z.; Feng, Q. Template-free synthesis of high specific surface area gauze-like porous graphitic carbon nitride for efficient photocatalytic degradation of tetracycline hydrochloride. *J. Mater. Sci.* **2021**, *56*, 4641–4653. [CrossRef]
44. Zhao, L.; Guo, L.; Tang, Y.; Zhou, J.; Shi, B. Novel g-$C_3N_4$/C/$Fe_2O_3$ Composite for Efficient Photocatalytic Reduction of Aqueous Cr (VI) under Light Irradiation. *Ind. Eng. Chem. Res.* **2021**, *60*, 13594–13603. [CrossRef]
45. Padhi, D.K.; Parida, K. Facile fabrication of α-FeOOH nanorod/RGO composite: A robust photocatalyst for reduction of Cr(VI) under visible light irradiation. *J. Mater. Chem. A* **2014**, *2*, 10300–10312. [CrossRef]